ACS OMEGA

http://pubs.acs.org/journal/acsodf

Article

Diatomite Composited with a Zeolitic Imidazolate Framework for Removing Phosphate from Water

Zicheng Chen, Huiwen Zhang, Guangyuan Fan, Xiangyang He, Zhibin He, and Lanhe Zhang*

Cite This: *ACS Omega* 2022, 7, 26154−26164

Read Online

ACCESS | Metrics & More | Article Recommendations

ABSTRACT: Adsorption technology based on various adsorbents has been widely applied in wastewater treatment containing phosphate. A novel diatomite adsorbent composited with ZIF-8 (CZD) was developed for removing phosphate from water in this work. The chitosan was used to pre-modify the diatomite so that ZIF-8 could be anchored on the surface of the diatomite solidly and uniformly. The diatomite composited with ZIF-8 was then used to remove phosphate in water by an adsorption process, the process variables such as adsorption time, temperature, pH, and competitive ions were investigated. The electrostatic attraction was the primary mechanism of phosphate removal. The adsorption reached equilibrium within 90 min, and its sorption capacity increased when adsorption time and temperature increased. Especially, CZD had a rapid adsorption rate and 85% of the phosphate in the solution can be adsorbed within the first 10 min. The maximum phosphate adsorption capacities of the modified diatomite reached 13.46, 13.55, and 13.95 mg/g at 25, 35, and 45 °C, respectively. The removal efficiencies of CZD for phosphate were more than 98% and even came up to 100% at 45 °C. The adsorption isotherms fit well with the Langmuir isotherm model. The Freundlich isotherm and Temkin isotherm showed that the adsorption process is physical in nature. The kinetic data of the adsorption process were fitted by the pseudo-second-order kinetics. Thermodynamic parameters indicated that the adsorption process was endothermic. This adsorbent provided an alternative for phosphate removal on account of the high adsorption efficiency in a short time. Therefore, CZD could be a promising and eco-friendly phosphate adsorbent for wastewater treatment.

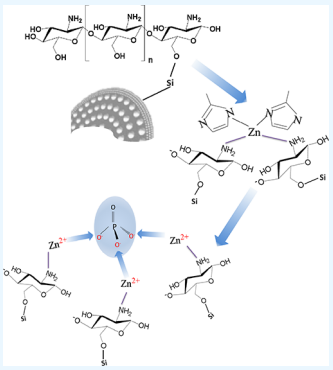

1. INTRODUCTION

Phosphorus is one of the essential elements for various life activities of human beings, animals, and plants.[1−3] It plays a critical role in agronomic production and industry development.[4] However, excess phosphorus emissions will lead to a series of environmental problems.[5] The accumulation of phosphorus in water from mining, industrial production, and agricultural activities could contribute to eutrophication.[6] Thus, phosphorus pollution has become one of the most critical factors toward ecological issues in the world.[7−11] Eutrophication may lead to a drastic decrease of dissolved oxygen in the absence of sunlight and the depopulation of aquatic species.[12,13] Since phosphorus is the minimum limiting factor for eutrophication, removing phosphorus in the water body becomes a vital strategy for controlling eutrophication.[14] Several practical techniques such as chemical precipitation, biological treatment, adsorption, and membrane separation have been used to remove phosphorus from wastewater.[15]

Compared with the other phosphorus removal methods, adsorption technology has been widely concerned by researchers owing to its simple operation, low cost, and high efficiency.[16,17] Various materials, such as clay minerals, carbonate minerals, steel slag, and red mud, have been developed as adsorbing materials of dephosphorization.[18−21] Limestone, fly ash, calcite, *etc.* were also used to control eutrophication by removal of phosphate. However, some adsorbents have been restricted because of low capacities for adsorption or the toxic compounds they released during the adsorption process.[22]

Diatomite, also known as diatomaceous earth, is a natural material derived from the fossilized remains of diatoms, which are widely distributed in seas or lakes and deposited at the bottom of water bodies after death.[23] According to the mineralogical classification, diatomite is non-crystalline opal-A and is mainly composed of amorphous hydrated silica ($SiO_2 \cdot nH_2O$).[24] Due to its unique physical and chemical characteristics, such as high mechanical strength, low density, and natural pores, we can find its applications in varied areas, such as a filtration aid, a flame retardant, a mild abrasive in products including metal polishes and toothpaste, an insecticide, an absorbent for liquids, a reinforcing filler in plastics and rubber, an antiblock in plastic films, a porous support for chemical

Received: March 18, 2022
Accepted: June 29, 2022
Published: July 18, 2022

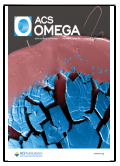

ACS Publications

© 2022 The Authors. Published by American Chemical Society

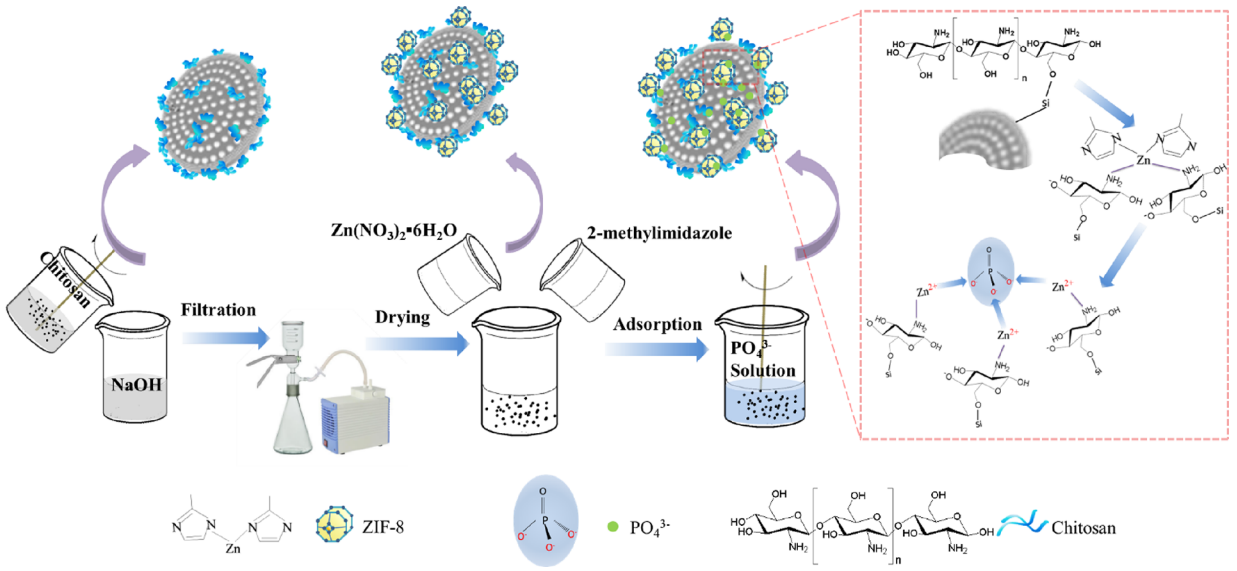

Figure 1. Schematic diagram of the preparation of adsorbents and adsorbing phosphate.

catalysts, a stabilizing component of dynamite, a thermal insulator, and an interior decoration material.[25−30] Diatomite has been approved as a food-grade material by the FDA (the U.S. Food and Drug Administration).[23] However, the PO_4^{3-} adsorption capacity of natural diatomite could not be competitive compared with other industrial adsorption materials because of the blocked channels and lower specific surface area. Hence, it is an excellent strategy to combine the diatomite with other functional materials to improve its adsorption performance.

The zeolitic imidazolate framework (ZIF-8), a sub-family of porous metal−organic frameworks, has identical topologies to conventional zeolites.[31] It has tunable porosity and superior thermal and chemical stabilities, potentially valuable for many applications. When ZIF-8 was used in phosphate removal from wastewater, the agglomeration of ZIF-8 particles with a nanoscale size resulted in a remarkable deterioration of adsorption efficiency.[32] As far as we know, it is not reported to remove phosphate in water using diatomite composited with MOFs. Thus, it may be a practical approach to composite ZIF-8 and the diatomite to prepare a novel absorbent.

In the present work, chitosan was used for diatomite pretreatment, considering the chemical inertness of diatomite. The functional groups of chitosan, such as amino and hydroxyl groups, will contribute to the loading of ZIF-8 on the surface of diatomite and make the distribution of ZIF-8 more evenly.

The phosphate removal performance of the composited diatomite was investigated in detail by the kinetics, thermodynamics, and equilibrium adsorption isotherm. We also studied the effect of process variables such as competitive anions, ionic strength, and solution pH on phosphate removal. Furthermore, the phosphate adsorption mechanism of the composited diatomite was studied. Due to the high adsorption efficiency of CZD in a short time, it could be a prospective adsorbent for water treatment.

2. MATERIALS AND METHODS

2.1. Materials. All chemicals were of analytical reagent grade. Monopotassium phosphate (KH_2PO_4), sodium hydroxide (NaOH), sodium carbonate (Na_2CO_3), potassium nitrate (KNO_3), potassium chloride (KCl), chitosan (90% of deacetylation degree), zinc nitrate hexahydrate, 2-methylimidazole, and methanol were purchased from Tianjin Kermel chemical reagent Co., Ltd. (Tianjin, China). Diatomite (D) was purchased from Tianjin Damao Chemical Reagent Co., Ltd. (Tianjin, China).

2.2. Preparation of Diatomite Coated with Chitosan. First, chitosan (0.18 g) was dissolved in 50 mL of acetic acid solution (5% v/v) and filtered for use. Diatomite (2.0 g) was immersed in the above chitosan solution for 10 min at room temperature. Then, the mixture was rapidly poured into 50 mL of NaOH aqueous solution (5 wt %) and dispersed for 10 min under stirring. Finally, the diatomite coated with chitosan (CMD) was obtained by rinsing the mixture with deionized water, filtration, and air drying.

2.3. Loading of ZIF-8 on the Surface of CMD. In a typical process, zinc nitrate hexahydrate (0.64 g) and 2-methylimidazole (0.72 g) were dissolved in 50 mL of methanol, respectively. The former solution was mixed with CMD for 20 min under stirring. The later solution was subsequently poured into the mixture, and they were dispersed for another 20 min under stirring and then kept overnight. The resultant mixture was washed throughout with deionized water, then filtered, and dried in an air oven with a temperature of 105 °C. The final product was chitosan-ZIF-8-modified diatomite (CZD). The process of CZD preparation and adsorbing phosphorus is shown in Figure 1.

2.4. Characterizations. The crystalline phase of the samples was characterized by an X-ray diffraction diffractometer (Maxima X XRD-7000, S/L, Shimadzu, Japan) with Cu Kα radiation (λ = 1.5418 Å, 30 mA, 40 kV) over the 2θ range of 5−80°. Scanning electron microscopy (SEM) was carried out using a FEG-SEM microscope (XL-30, FEI company, USA). The distribution of the elements was examined by energy-dispersive X-ray spectroscopy (EDS, X-MAX, Oxford Instruments, UK). Fourier-transform infrared (FT-IR) spectra were recorded using a Fourier-Transform infrared spectrometer (VERTEX 70, Germany). The element content of Zn in the composite was measured by an inductively coupled plasma optical emission spectrometer (ICP-OES, Thermo-Scientific iCAP6300, USA).

2.5. Adsorption Kinetics. CZD (0.2 g) was added into 50 mL of aqueous solution of phosphate (10 mg/L) in an

https://doi.org/10.1021/acsomega.2c01648
ACS Omega 2022, 7, 26154−26164

Erlenmeyer flask, and the mixture was shaken at 160 rpm in a mechanical shaker at 25 °C for a fixed period (2, 5, 10, 15, 30, 60, 90, 120, 180, 240, 360, and 480 min). Then, the mixtures were filtered, and phosphate concentrations of the filtrate were measured by a UV−vis spectrophotometer at 700 nm. The equations used are as follows:

The pseudo-first-order model:

$$\ln(q_e - q_t) = \ln q_e - k_1 t \quad (1)$$

The pseudo-second-order model:

$$\frac{t}{q_t} = \frac{1}{k_2 q_e^2} + \frac{t}{q_e} \quad (2)$$

where k_1 (min^{-1}) and k_2 (g mg^{-1} min^{-1}) were the pseudo-first-order and second-order kinetic rate constant, respectively; q_t (mg/g) is the PO_4^{3-} sorption capacity at time t, and q_e (mg/g) is the equilibrium adsorption capacity.[17]

2.6. Adsorption Isotherm. CZD (0.2 g) was mixed with phosphate solutions (50 mL) with different initial phosphate concentrations ranging from 5−90 mg/L, and the mixtures were shaken in a mechanical shaker (160 rpm) at 25, 35, and 45 °C, respectively. After 90 min of mixing, all the mixtures were filtered, and the phosphate concentrations of the filtrates were measured by a UV−vis spectrophotometer. The Langmuir, Freundlich, and Temkin models were used to investigate the adsorption isotherms of phosphate. The linear forms of Langmuir, Freundlich, and Temkin equations are given in eqs 3−5, respectively.

$$\frac{C_e}{q_e} = \frac{C_e}{q_m} + \frac{1}{K_L q_m} \quad (3)$$

$$\ln q_e = \ln K_F + \frac{1}{n} \ln C_e \quad (4)$$

$$q_e = B \ln K_T + B \ln C_e \quad (5)$$

where C_e (mg/L) is the equilibrium concentration of the phosphate solutions, and q_e (mg/g) and q_m (mg/g) are the equilibrium adsorption capacity and maximum adsorption capacity, respectively. K_L ((L/mg) and K_F ((mg/g) (L/mg)$^{1/n}$) are the Langmuir and Freundlich constants, respectively; $1/n$ is the Freundlich exponent (n is a measure of the deviation from the linearity of adsorption).[33] $B = RT/b$ is a constant related to the heat of sorption (J/mol); b is the Temkin isotherm constant (L/g); R is the ideal gas constant (8.314 J/(mol·K)); T is the thermodynamic absolute temperature (K).[34]

2.7. Adsorption Thermodynamics. Thermodynamic characteristics were investigated to further evaluate the adsorption process such as exothermic or endothermic. Thermodynamic parameters including $\Delta G°$ (Gibbs free energy), $\Delta H°$ (enthalpy), and $\Delta S°$ (entropy) were calculated using the isotherm data by the following van't Hoff equation:

$$\Delta G° = -RT \ln K_d \quad (6)$$

$$\ln K_d = \frac{\Delta S°}{R} - \frac{\Delta H°}{RT} \quad (7)$$

where R is the universal gas constant (R = 8.314 J/mol·K), T is the absolute temperature (K), and K_d (L/mol) is the thermodynamic equilibrium constant calculated from the Langmuir equilibrium constant.

2.8. Effects of Environmental Conditions on Phosphate Removal. Chemical environments are the crucial factors that affect the adsorption ability of adsorbents, such as pH and anions. The effects of pH and competitive ions were evaluated in batch adsorption experiments. For the effect of initial pH, the adsorbents (0.2 g) were added into 50 mL of phosphate solutions (10 mg/L) with initial pH from 3−11 and shaken (160 rpm) at room temperature of 25 °C for 90 min. The pH value of the solutions was adjusted with 1 mol/L NaOH or acetic acid solution. For the effect of competitive anions (CO_3^{2-}, Cl^-, NO_3^-), 0.2 g of adsorbent was mixed with 50 mL of phosphate solution (10 mg/L), which contained one of the above anions and shaken at 160 rpm for 90 min. The concentrations of competitive ions varied within a specific range. All the suspensions were filtered, and the phosphate concentrations of the filtrates were measured by a UV−vis spectrophotometer. The equations of adsorption capacity (q_e) and efficiency (E_e) are expressed as follows:

$$q_e = \frac{(C_0 - C_e)V}{m} \quad (8)$$

$$E_e = \frac{C_0 - C_e}{C_0} \times 100\% \quad (9)$$

where C_0 (mg/L) and C_e (mg/L) are the initial and equilibrium solution concentrations, respectively; V (L) is the volume of the solution, and m (g) is the mass of the adsorbent.

3. RESULTS AND DISCUSSION

3.1. Characterizations. Figure 2 shows the FT-IR spectra of diatomite (D), chitosan, CMD, ZIF-8, and CZD samples. The peaks at 472 and 1092 cm^{-1} correspond to the asymmetric stretching vibration of Si−O−Si bonds, which proves the presence of SiO_2 in diatomite.[35−39] The FT-IR spectra of chitosan showed stretching vibration of carbonyl (C═O, amide I band) at 1652 cm^{-1} and the amino group (N−H, amide II band) at 1599 cm^{-1} and C−N (amide III band) at 1324 cm^{-1}, respectively. After diatomite was coated with chitosan, the corresponding characteristic peaks at 2919, 2851, and 1622 cm^{-1} appeared in the spectra of CMD, which indicated that chitosan had been covered on the surface of diatomite successfully. It can be seen that the characteristic peaks of synthesized ZIF-8 are in good agreement with the corresponding absorption spectra, which was reported in the previous literature.[40] The bands in the spectral region of 600−1500 cm^{-1} are assigned to the ring stretching or bending vibration of the imidazole ring. Furthermore, the peak at 420 cm^{-1} is associated with the Zn−N stretching vibration.[31,41] Due to the presence of chitosan, it is beneficial to the loading of ZIF-8. After modification, as seen from the spectrum of CZD, the characteristic peaks of ZIF-8 at 1578, 1458, 1419, 1174, and 693 cm^{-1} appeared at modified diatomite, which illustrated that ZIF-8 was successfully loaded on the surface of diatomite.

The XRD patterns of diatomite, chitosan, ZIF-8, and chitosan-ZIF-8-modified diatomite are shown in Figure 3. The diffraction spectrogram of Figure 3a indicates that the diatomite consists mainly of silica (SiO_2). As shown in Figure 3b, the characteristic peak of chitosan appears at about 2θ of 20°, which belongs to the monoclinic system. The XRD pattern of ZIF-8 is presented in Figure 3c, which is consistent with the simulated SOD-type ZIF-8 structure, confirming that the sample has a pure ZIF-8 phase.[41] As shown in Figure 3d, the characteristic peaks of

https://doi.org/10.1021/acsomega.2c01648
ACS Omega 2022, 7, 26154−26164

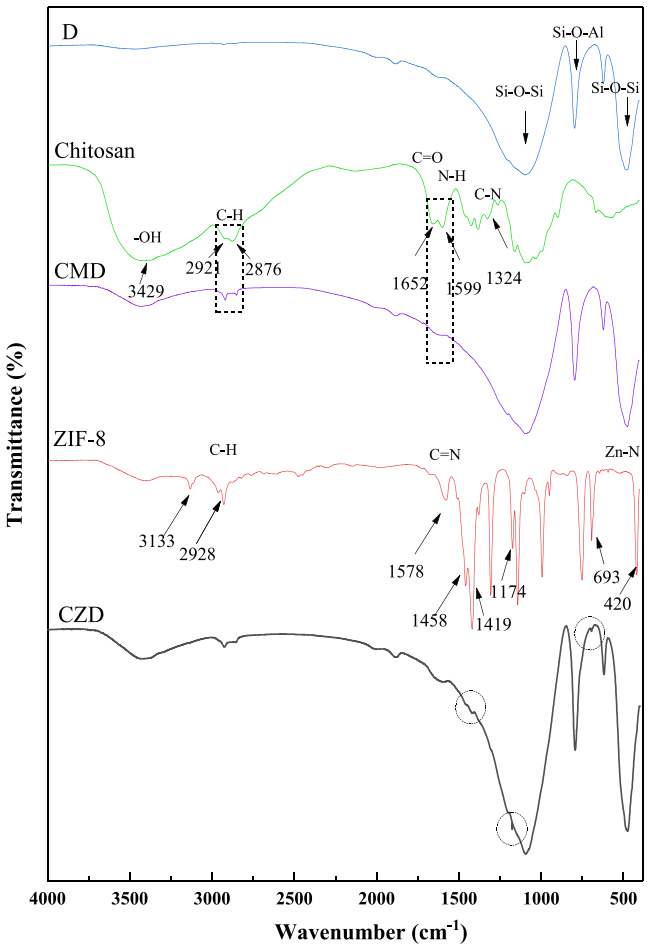

Figure 2. FT−IR spectra of samples.

ZIF-8 appeared in the pattern of CZD, which further confirmed that ZIF-8 was successfully loaded on the surface of the diatomite.

Figure 4 shows the scanning electron microscope (SEM) images of diatomite, CMD, and CZD. The natural diatomite's neat surface and clear pore structure can be observed in Figure 4a_1−a_3. When chitosan was coated onto the surface of diatomite, as schematically illustrated in Figure 4b, the surface of the diatomite seemed rougher than that of natural diatomite. It can be seen that the chitosan is uniformly coated in the outermost layer of the diatomite. After loading with ZIF-8, as shown in Figure 4c, ZIF-8 particles were evenly distributed on the surface of diatomite, forming a hierarchical pore structure. It could be expected to improve the adsorption performance of diatomite. It is clearly seen that the nanometer-sized crystals have uniform cubic shapes, which is consistent with the reported results.[42] As shown in Figure 4c_3, the size of ZIF-8 is about 70 nm.

An energy-dispersive X-ray spectrometer (EDS) analyzed the distribution of elements on modified diatomite. Figure 5 shows the EDS mapping of CZD with Si, O, N, and Zn. It was found that Zn and N were well dispersed on the silicon skeleton of diatomite. The uniformly existing Zn element indicated that ZIF-8 was evenly dispersed on the surface of diatomite. The EDS spectrum of CZD confirmed that diatomite was mainly composed of silicon and oxygen (SiO_2). The content of N and Zn of the CZD was 1.70% and 2.58%, respectively. Therein, the content of zinc was almost close to that of the ICP-OES analysis results, which is 5.53% (15,840 ppm) of the total mass.

3.2. Adsorption Results of D, CMD, and CZD. The phosphate adsorption capacity and adsorption efficiency of D, CMD, and CZD at different temperatures are presented in Figure 6. The adsorption capacity of D, CMD, and CZD increased with increasing phosphate concentration and close to equilibrium when the concentration was higher than 45 mg/L. It can be clearly seen that the adsorption capacity of diatomite after the modification has been significantly improved compared to D and CMD. The maximum capacity of CZD is 13.46 mg/g for phosphate removal, higher than those of CMD and D. The phosphate efficiency has an appreciable increase after loading ZIF-8 on the diatomite, as shown in Figure 6b. The removal efficiencies of CZD are more than 98%, and it comes up to 100% at 45 °C, in comparison with only 4.67% for D and 17.1% for CMD. The results showed that the adsorption capacity of diatomite was obviously improved after being modified with chitosan and ZIF-8. Table 1 shows the phosphate adsorption capacities of different adsorbents. The material produced in this paper is a good phosphorus adsorption material in terms of adsorption time and efficiency.

3.3. Effect of Initial pH. The effect of pH on phosphate adsorption by CZD is presented in Figure 7. CZD exhibits a low adsorption capacity at pH = 0−4 because the phosphate species mainly are composited with H_3PO_4 and $H_2PO_4^-$, and the electrostatic effect between phosphate and CZD is weak.[22] The phosphate removal capacity increased with the initial solution pH from 4 to 6, and phosphate adsorption exhibited the largest capacity (7.48 mg/g) at an initial pH of 5.81. It can be attributed that ZIF-8 has the highest positive zeta potential values at pH = 4−8.[47] Meanwhile, this sorption behavior can also be explained by PO_4^{x-} species changing in the case of pH = 4−8.[22] With the increase of pH, the solution's existing phosphorus form gradually changed from H_3PO_4 to $H_2PO_4^-$, HPO_4^{2-}, and PO_4^{3-}.[48] As pH continued to rise, the negative charge of phosphate increased. However, the zeta potential of ZIF-8 dropped dramatically, resulting in a decline in the adsorption capacity. In the meantime, OH^- competed with phosphate species and binding to the active adsorption sites, further reducing the adsorption capacity. It can be speculated that when the pH is below 5, the adsorption behavior of CZD is dominated by the phosphate species; when the pH is above 8, the adsorption behavior of CZD is dominated by the electrical charge of CZD. The adsorbent works best under neutral and near-neutral conditions, conducive to its practical application in phosphorus wastewater treatment and phosphorus recovery.

3.4. Effect of Competitive Anions. The coexistence of CO_3^{2-}, Cl^-, and NO_3^- may typically compete with phosphate in wastewater during the adsorption process.[49] They can interfere with the absorption of phosphate through competitive adsorption and reduce the efficiency of P removal. The influence of the competitive anions on phosphate adsorption is shown in Figure 8. It showed that Cl^- and NO_3^- had a little competitive effect for PO_4 removal. Specifically, the effect of Cl^- was nearly negligible when it was kept at a low concentration. CO_3^{2-} impacted significantly on phosphate removal, with adsorption efficiency decreasing from 85.93% to 55.24% because CO_3^{2-} might interact with the active site and compete with phosphate.[17] Moreover, the negative effect was proportional to the concentration of competitive anions. In a word, the impact of the above anions on phosphate adsorption followed a descending order as $CO_3^{2-} > NO_3^- > Cl^-$.

3.5. Adsorption Kinetics. The phosphate adsorption capacities of CZD were expressed as a function of contact

https://doi.org/10.1021/acsomega.2c01648
ACS Omega 2022, 7, 26154−26164

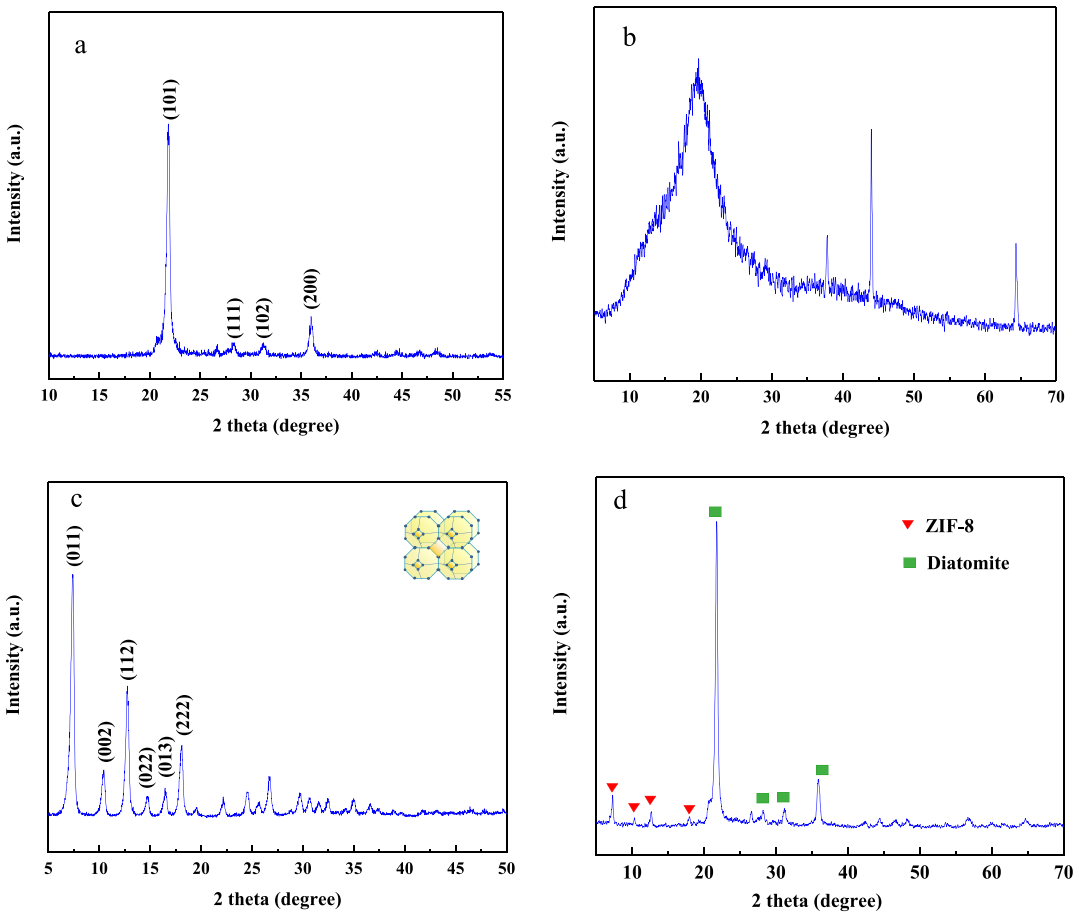

Figure 3. XRD pattern of (a) diatomite, (b) chitosan, (c)ZIF-8, and (d) CZD.

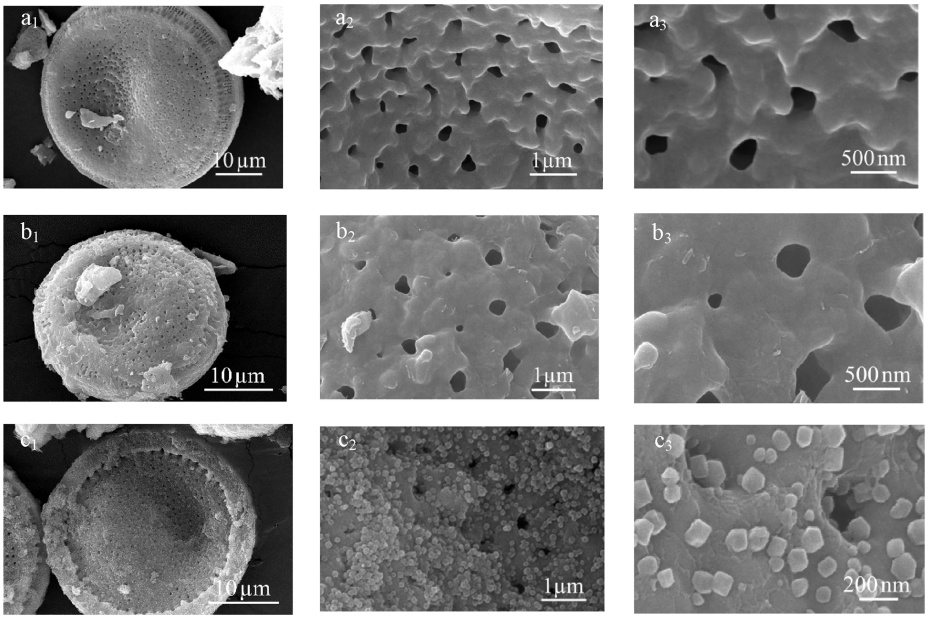

Figure 4. SEM images of (a) D, (b) CMD, and (c) CZD.

time. As shown in Figure 9, phosphate sorption increased rapidly and was close to equilibrium within 90 min and then remained comparatively stable. The results revealed that a short time is required for CZD to remove phosphate effectively. 85% of the phosphate in the solution even can be adsorbed within 10 min.

The kinetic adsorption results have been analyzed using pseudo-first-order and pseudo-second-order models (Figure 10). As seen from the kinetic parameters in Table 2, the correlation coefficients of the pseudo-second-order model (R^2 = 0.999) were more significant than the pseudo-first-order model (R^2 =

https://doi.org/10.1021/acsomega.2c01648
ACS Omega 2022, 7, 26154−26164

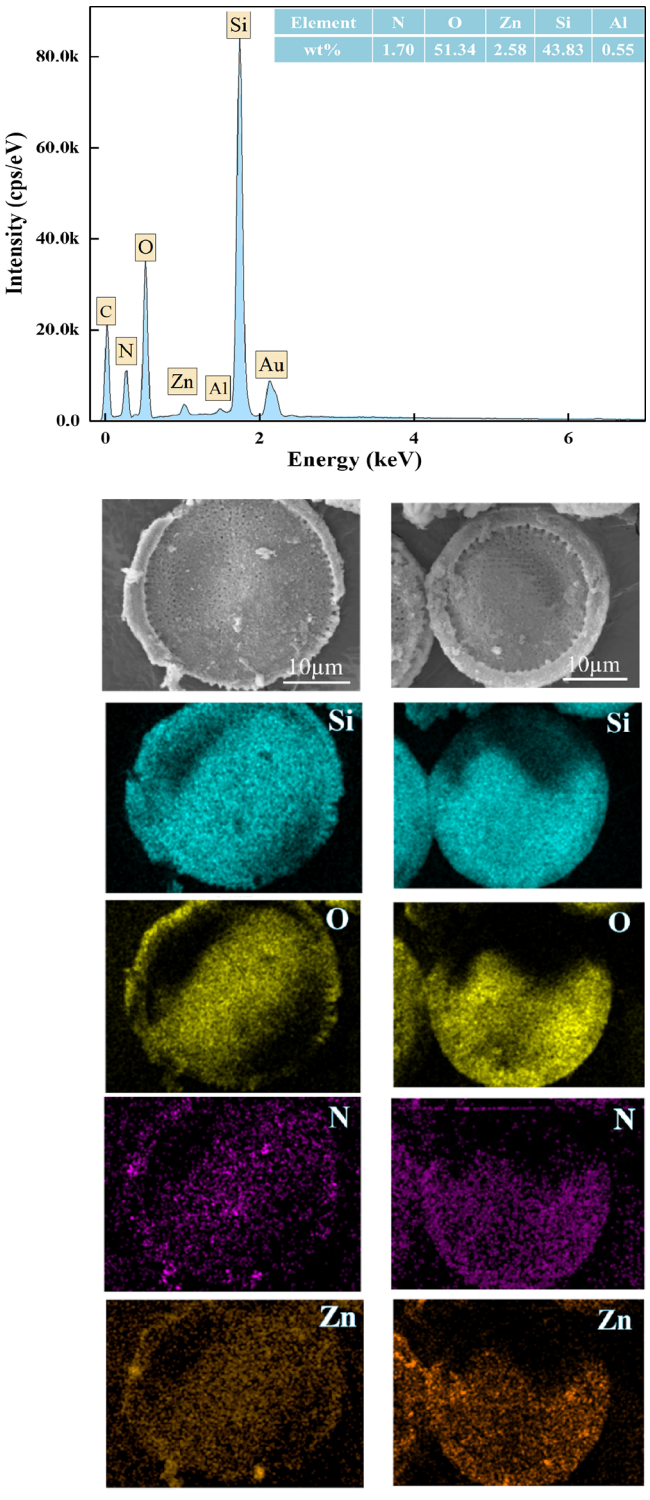

Figure 5. EDS spectrum of CZD and element maps of Si, O, N, and Zn.

0.825). This result is similar to the previous kinetic results obtained for various adsorbent-pollutant systems.[50,51] Furthermore, the calculated value of equilibrium adsorption of CZD to phosphorus is close to the experimental results. Thus, the adsorption kinetics of phosphorus coincides with the pseudo-second-order model for the entire adsorption period.

The intraparticle diffusion model was used to define the rate-limiting step of the adsorption process.[52] As can be seen from Figure 11, the kinetics adsorption of phosphate consists of three consecutive phases: bulk diffusion, film diffusion, and pore diffusion.[34] The first stage observed at $1.4 < t^{0.5} < 3.9$ $min^{0.5}$ was rapid, the rate slowed down slightly in the second phase, and equilibrium was established at the third stage. The diffusion of phosphate molecules through pores to the active sites of CZD at the third phase. If the linear plot of q_t versus $t^{0.5}$ passed through the origin, then intraparticle diffusion was the only rate-limiting step.[52] However, the lines in Figure 11 did not pass through the origin, indicating that the adsorption process was governed not only by intraparticle diffusion as the rate-limiting step but also by other factors in the adsorption process.

3.6. Adsorption Isotherms. In this study, the equilibrium adsorption of phosphate by CZD was investigated using Langmuir, Freundlich, and Temkin isotherm models. The isotherm curves and corresponding parameters are summarized in Figure 12 and Table 3. According to the results, the Langmuir model provided a higher correlation coefficient value compared to the other two isotherm models. Thus, the Langmuir isotherm model is the best-fitted model to describe the adsorption behavior of phosphate adsorption. Based on the R^2 values, the correlate order was as follows: Langmuir (R^2 = 0.9866−0.9887) > Freundlich (R^2 = 0.9634−0.9768) > Temkin (R^2 = 0.8817−0.9087). It was indicated that the monolayer adsorption of phosphate molecules occurred on the heterogeneous surface of CZD.[53] The obtained isotherm results are in agreement with the previous studies.[54,55] In the Freundlich isotherm, the significance of the n value is as follows: adsorption is linear if $n = 1$; adsorption is physisorption if $n > 1$; adsorption is chemisorption if $n < 1$.[56] In this work, $n > 1$ can indicate that the adsorption process is physical. In Temkin isotherm, B is 1.99−2.26 J/mol, which proved that the adsorption reaction occurred endothermically and the adsorption is physical in nature.[57−59]

Furthermore, the maximum adsorption capacity of CZD based on the fitting results of the Langmuir model was 14.27 mg/g at 25 °C, which is four times more than the original diatomite. Also, the adsorption capacity increased with the increase of reaction temperature, indicating that a higher temperature is beneficial to the adsorption of phosphate. It is also consistent with the result of adsorption thermodynamics.

3.7. Adsorption Thermodynamics. The changes in the Gibbs free energy ($\Delta G°$), enthalpy ($\Delta H°$), and entropy ($\Delta S°$) were determined in accordance with study results of temperature effect (Table 4). The values of $\Delta H°$ and $\Delta S°$ were obtained from the intercept and slope of the line in Figure 13. The $\Delta G°$ values were negative at different temperatures, indicating that the adsorption process was favorable and spontaneous. As the reaction temperature increased, the value of $\Delta G°$ decreased gradually, indicating that the temperature in the system had a certain influence on the adsorption process. The higher temperature was more favorable to the forward reaction and can promote the adsorption process. The values of $\Delta H°$ were positive at different temperatures, indicating that the adsorption process was endothermic.[60] The adsorption efficiency of the adsorbent increased with increasing temperature; hence, a higher temperature was more conducive to the reaction. The positive value of $\Delta S°$ indicated that the randomness in the system increased with the progress of the adsorption process, which is conducive to the adsorption effect of the adsorbent for phosphate.

4. CONCLUSIONS

Chitosan-ZIF-8-modified diatomite, prepared via a simple process, exhibited an excellent affinity to phosphate in an

https://doi.org/10.1021/acsomega.2c01648
ACS Omega 2022, 7, 26154−26164

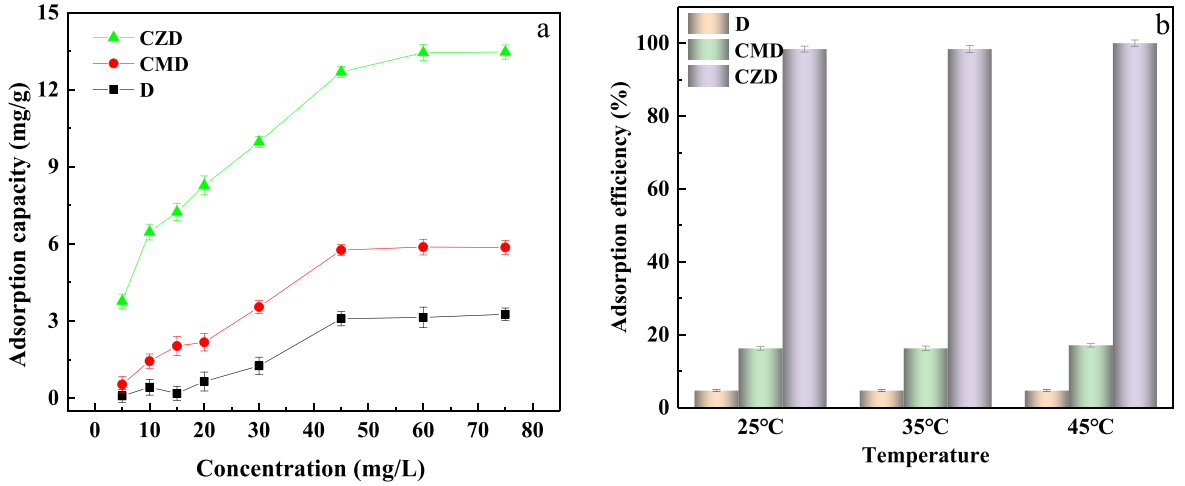

Figure 6. (a) Adsorption capacity of D, CMD, and CZD in different phosphate concentrations; (b) adsorption efficiency of D, CMD, and CZD for 5 mg/L phosphate solution at different temperatures (the time of absorbing is 90 min).

Table 1. Comparison of the Phosphate Adsorption Capacities of Various Adsorbents

adsorbents	equilibrium time	adsorption capacity (mg/g)	ref
Fe(III)-doped chitosan	48 h	15.7	43
Fe−Mn oxide adsorbent	24 h	18.4	44
magnetic illite clay	90 min	5.48	45
Fe^0/iron oxide-DE	30 min	37.0	46
0.05-HIOMD (hydrous iron oxide modified diatomite)	24 h	4.89	14
CZD	90 min	13.95	This work

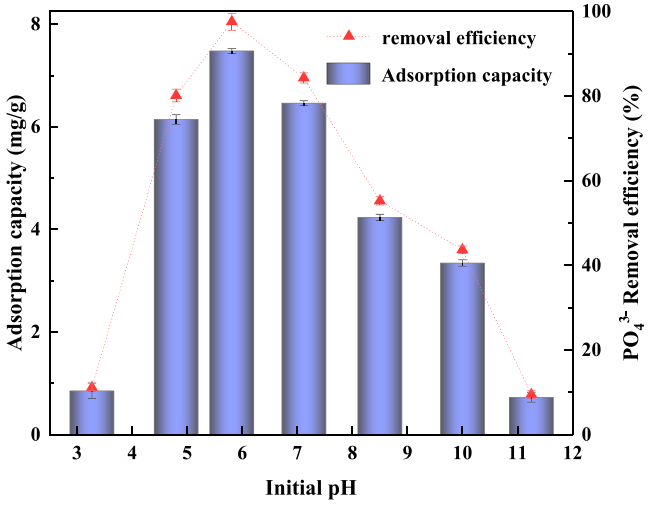

Figure 7. Effect of initial solution pH for adsorption capacity of CZD.

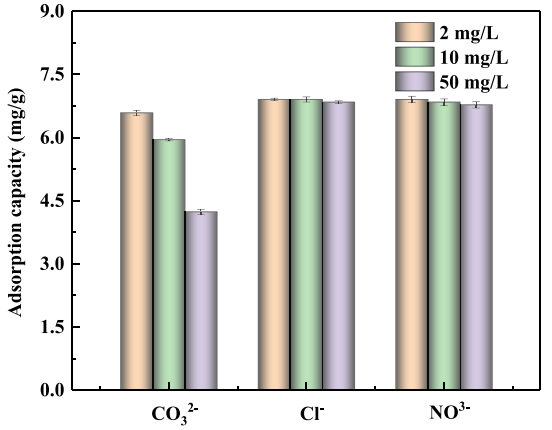

Figure 8. Effect of competitive anions on phosphate adsorption (adsorbent dosage = 0.2 g, temperature = 25 °C).

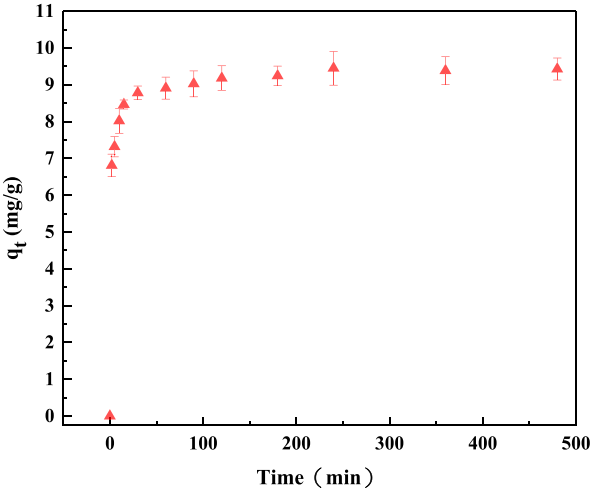

Figure 9. Effect of contact time on the phosphate sorption of CZD.

aqueous solution. It possessed high adsorption efficiency at a low concentration, and the value of q_m calculated by the Langmuir isotherm equation was 14.58 mg/g at 45 °C. The removal efficiencies of CZD to phosphate were more than 98%. The pH value of the solution had a significant influence on phosphate adsorption, and optimal removal was at pH 5.81. The phosphate adsorption isotherm was fitted better with the Langmuir model than the Freundlich model, and the kinetic data followed the pseudo-second-order model. Thermodynamic parameters indicated that the adsorption process was endothermic, and a higher temperature was more conducive to the reaction. The Freundlich isotherm and Temkin isotherm showed that the adsorption process is physical in nature. Moreover, electrostatic interaction is the primary mechanism of phosphate removal.

https://doi.org/10.1021/acsomega.2c01648
ACS Omega 2022, 7, 26154−26164

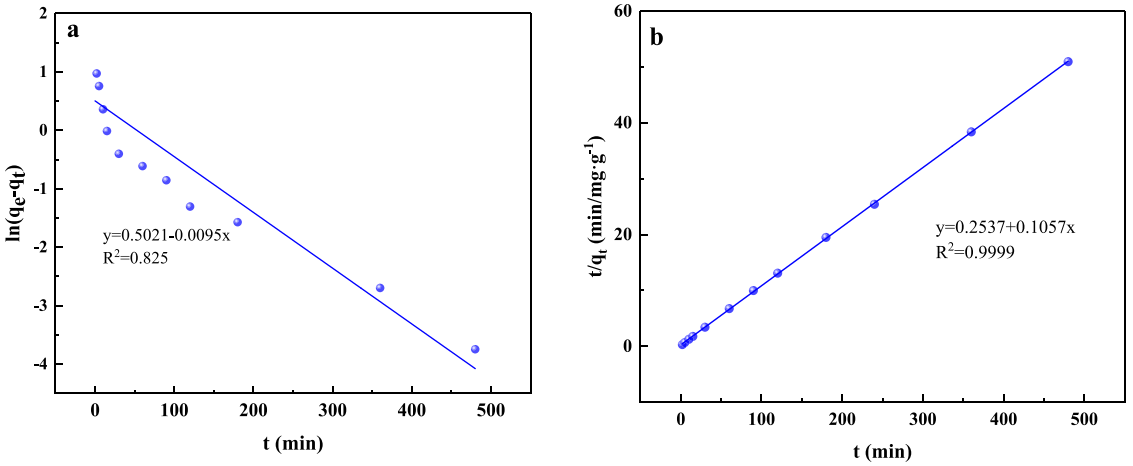

Figure 10. Adsorption kinetics of phosphate adsorption. (a) Pseudo-first-order kinetics. (b) Pseudo-second-order kinetics.

Table 2. Kinetic Parameters and Regression Coefficients for the Adsorption of Phosphate onto CZD

		pseudo-first-order			pseudo-second-order		
C_0 (mg/L)	$q_{e,exp}$ (mg/g)	k_1 (min^{-1})	$q_{e,cal}$ (mg/g)	R^2	k_2 (g/(mg·min))	$q_{e,cal}$	R^2
10	9.45	0.0095	1.65	0.825	0.0506	9.46	0.999

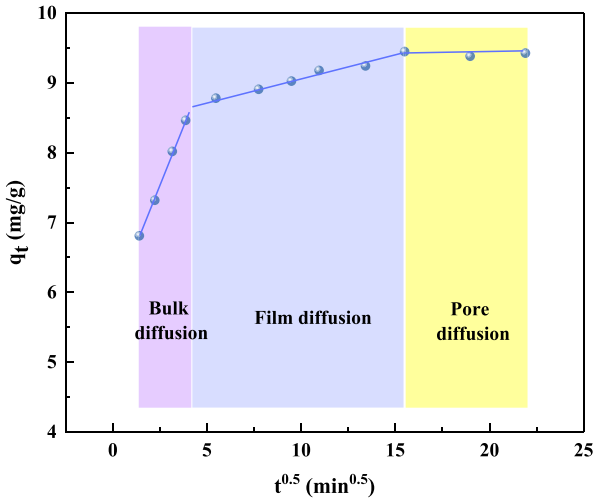

Figure 11. Intraparticle diffusion kinetic plots for phosphate adsorption onto CZD.

The present study demonstrated that CZD is expected to be an alternative as an adsorbent for phosphorus removal.

AUTHOR INFORMATION

Corresponding Author

Lanhe Zhang − *School of Chemical Engineering, Northeast Electric Power University, Jilin, Jilin 132012, P. R. China*; Email: zhanglanhe@163.com

Authors

Zicheng Chen − *School of Chemical Engineering, Northeast Electric Power University, Jilin, Jilin 132012, P. R. China; Department of Chemical Engineering, University of New Brunswick, Fredericton, NB E3B 5A3, Canada*; orcid.org/0000-0002-1962-9373

Huiwen Zhang − *School of Chemical Engineering, Northeast Electric Power University, Jilin, Jilin 132012, P. R. China*

Guangyuan Fan − *School of Chemical Engineering, Northeast Electric Power University, Jilin, Jilin 132012, P. R. China*

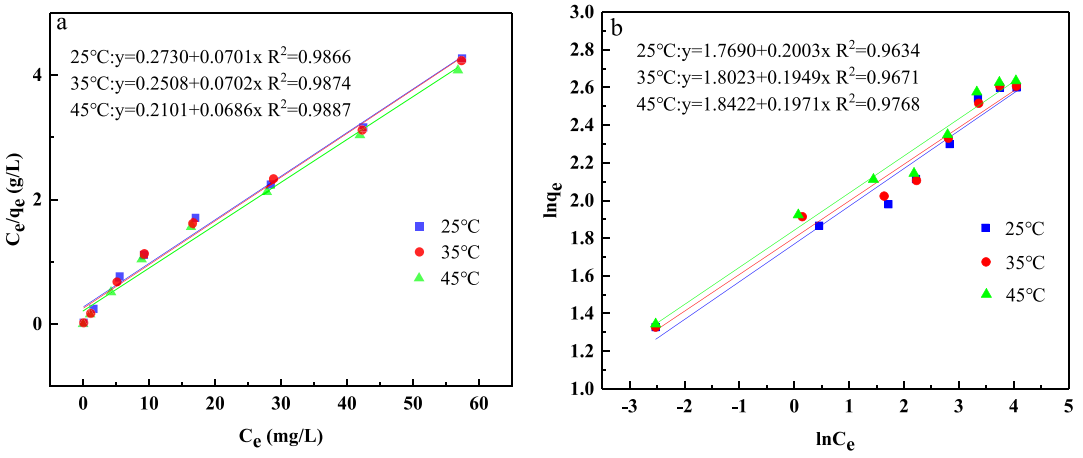

Figure 12. Langmuir (a) and Freundlich (b) model fit of adsorption isotherm data points of phosphate.

https://doi.org/10.1021/acsomega.2c01648
ACS Omega 2022, 7, 26154−26164

Table 3. Isotherm Parameters for Phosphate Adsorption onto CZD

	Langmuir			Freundlich			Temkin		
temperature (°C)	K_L (L/mg)	q_m (mg/g)	R^2	K_F ((mg/g) (L/mg)$^{1/n}$)	n	R^2	B (J/mol)	K_T (J/mol)	R^2
25	0.26	14.27	0.9866	5.87	4.99	0.9634	2.261	6.66	0.9087
35	0.28	14.25	0.9874	6.06	5.13	0.9671	1.988	13.85	0.8817
45	0.33	14.58	0.9887	6.31	5.07	0.9768	1.989	17.69	0.9002

Table 4. Parameters of Adsorption Thermodynamics with CZD

T (K)	K_d (L/mol)	$\Delta G°$ (kJ/mol)	$\Delta S°$ (kJ/mol·K)	$\Delta H°$ (kJ/mol)
298.15	24420.02	−25.04		
308.15	26560.42	−26.10	0.12	10.30
318.15	31746.03	−27.42		

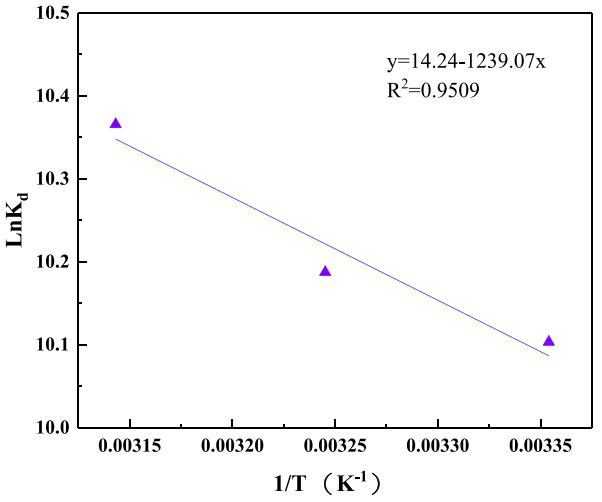

Figure 13. Linear plot of lnK_d vs 1/T.

Xiangyang He − *School of Chemical Engineering, Northeast Electric Power University, Jilin, Jilin 132012, P. R. China*
Zhibin He − *Department of Chemical Engineering, University of New Brunswick, Fredericton, NB E3B 5A3, Canada*

Complete contact information is available at: https://pubs.acs.org/10.1021/acsomega.2c01648

Notes

The authors declare no competing financial interest.

■ ACKNOWLEDGMENTS

The authors are grateful for the support of the Science and Technology Development Plan of Jilin Provence of the People's Republic of China. (Grant No. 20190303065SF).

■ REFERENCES

(1) Koh, K. Y.; Chen, Z.; Zhang, S.; Paul Chen, J. Cost-effective phosphorus removal from aqueous solution by a chitosan/lanthanum hydrogel bead: Material development, characterization of uptake process and investigation of mechanisms. *Chemosphere* **2022**, *286*, 131458−131468.
(2) De-Bashan, L. E.; Bashan, Y. Recent advances in removing phosphorus from wastewater and its future use as fertilizer (1997−2003). *Water Res.* **2004**, *38*, 4222−4246.
(3) Xia, P.; Wang, X. J.; Wang, X.; Zhang, J. Synthesis and characterization of MgO modified diatomite for phosphorus recovery in eutrophic water. *J. Chem. Eng. Data* **2016**, *62*, 226−235.
(4) He, H.; Zhang, N.; Chen, N.; Lei, Z.; Zhang, Z. Efficient phosphate removal from wastewater by MgAl-LDHs modified hydrochar derived from tobacco stalk. *Bioresour. Technol. Rep.* **2019**, *8*, 100348−100356.
(5) Carleton, G.; Glowczewski, J.; Cutright, T. Design and preliminary testing of an in-field passive treatment system for removing phosphorus from surface water. *Appl. Sci.* **2021**, *11*, 3743−3758.
(6) Ding, Y.; Sabatini, D. A.; Butler, E. C. Phosphorus recovery and recycling from model animal wastewaters using materials prepared from rice straw and corn cobs. *Water Sci. Technol.* **2021**, *83*, 1893−1906.
(7) Loganathan, P.; Vigneswaran, S.; Kandasamy, J.; Bolan, N. S. Removal and recovery of phosphate from water using sorption. *Crit. Rev. Environ. Sci. Technol.* **2014**, *44*, 847−907.
(8) Song, Y.; Yuan, P.; Wei, Y.; Liu, D.; Wu, H. Constructing hierarchically porous nest-like Al_2O_3-MnO_2@diatomite composite with high specific surface area for efficient phosphate removal. *Ind. Eng. Chem. Res.* **2019**, *58*, 23166−23174.
(9) Huang, Y.; Yang, J.-K.; Keller, A. A. Removal of arsenic and phosphate from aqueous solution by metal (hydr-) oxide coated sand. *ACS Sustainable Chem. Eng.* **2014**, *2*, 1128−1138.
(10) Lyngsie, G.; Borggaard, O. K.; Hansen, H. C. B. A three-step test of phosphate sorption efficiency of potential agricultural drainage filter materials. *Water Res.* **2014**, *51*, 256−265.
(11) Wu, Y.; Li, X.; Yang, Q.; Wang, D.; Xu, Q.; Yao, F.; Chen, F.; Tao, Z.; Huang, X. Hydrated lanthanum oxide-modified diatomite as highly efficient adsorbent for low-concentration phosphate removal from secondary effluents. *J. Environ. Manage.* **2019**, *231*, 370−379.
(12) Bacelo, H.; Pintor, A. M. A.; Santos, S. C. R.; Boaventura, R. A. R.; Botelho, C. M. S. Performance and prospects of different adsorbents for phosphorus uptake and recovery from water. *Chem. Eng. J.* **2020**, *381*, 122566−122584.
(13) Xia, P.; Wang, X.; Wang, X.; Song, J.; Wang, H.; Zhang, J.; Zhao, J. Struvite crystallization combined adsorption of phosphate and ammonium from aqueous solutions by mesoporous MgO−loaded diatomite. *Colloids Surf., A* **2016**, *506*, 220−227.
(14) Wang, Z.; Lin, Y.; Wu, D.; Kong, H. Hydrous iron oxide modified diatomite as an active filtration medium for phosphate capture. *Chemosphere* **2016**, *144*, 1290−1298.
(15) Bui, T. H.; Hong, S. P.; Yoon, J. Development of nanoscale zirconium molybdate embedded anion exchange resin for selective removal of phosphate. *Water Res.* **2018**, *134*, 22−31.
(16) Zhang, B.; Wang, X.; Li, S.; Liu, Y.; An, Y.; Zheng, X. Preferable adsorption of nitrogen and phosphorus from agricultural wastewater Using thermally modified zeolite−diatomite composite adsorbent. *Water* **2019**, *11*, 2053−2064.
(17) Jia, X.; He, X.; Han, K.; Ba, Y.; Zhao, X.; Zhang, Q. La_2O_3-modified MCM-41 for efficient phosphate removal synthesized using natural diatomite as precursor. *Water Sci. Technol.* **2019**, *79*, 1878−1886.
(18) Xie, J.; Wang, Z.; Lu, S.; Wu, D.; Zhang, Z.; Kong, H. Removal and recovery of phosphate from water by lanthanum hydroxide materials. *Chem. Eng. J.* **2014**, *254*, 163−170.
(19) Yan, L. G.; Xu, Y. Y.; Yu, H. Q.; Xin, X. D.; Wei, Q.; Du, B. Adsorption of phosphate from aqueous solution by hydroxy-aluminum, hydroxy-iron and hydroxy-iron-aluminum pillared bentonites. *J. Hazard. Mater.* **2010**, *179*, 244−250.
(20) Xu, N.; Li, Y.; Zheng, L.; Gao, Y.; Yin, H.; Zhao, J.; Chen, Z.; Chen, J.; Chen, M. Synthesis and application of magnesium amorphous calcium carbonate for removal of high concentration of phosphate. *Chem. Eng. J.* **2014**, *251*, 102−110.

(21) Xiong, W.; Peng, J. Development and characterization of ferrihydrite-modified diatomite as a phosphorus adsorbent. *Water Res.* **2008**, *42*, 4869−4877.
(22) Xie, F.; Wu, F.; Liu, G.; Mu, Y.; Feng, C.; Wang, H.; Giesy, J. P. Removal of phosphate from eutrophic lakes through adsorption by in situ formation of magnesium hydroxide from diatomite. *Environ. Sci. Technol.* **2014**, *48*, 582−590.
(23) Jang, M.; Min, S. H.; Kim, T. H.; Park, J. K. Removal of arsenite and arsenate using hydrous ferric oxide incorporated into naturally occurring porous diatomite. *Environ. Sci. Technol.* **2006**, *40*, 1636−1643.
(24) Elmas, N.; Bentli, I. Environmental and depositional characteristics of diatomite deposit, Alayunt Neogene Basin (Kutahya), West Anatolia, Turkey. *Environ. Earth Sci.* **2013**, *68*, 395−412.
(25) Chen, Y.; Wu, Q.; Zhou, C.; Jin, Q. Enhanced photocatalytic activity of La and N co-doped TiO_2/diatomite composite. *Powder Technol.* **2017**, *322*, 296−300.
(26) Zong, P.; Makino, D.; Pan, W.; Yin, S.; Sun, C.; Zhang, P.; Wan, C.; Koumoto, K. Converting natural diatomite into nanoporous silicon for eco-friendly thermoelectric energy conversion. *Mater. Des.* **2018**, *154*, 246−253.
(27) Lauermannova, A.; Lojka, M.; Jankovsky, O.; Faltysova, I.; Pavlıkova, M.; Pivak, A.; Zaleska, M.; Pavlık, Z. High-performance magnesium oxychloride composites with silica sand and diatomite. *J. Mater. Res. Technol.* **2021**, *11*, 957−969.
(28) Li, C.; Sheng, X.; Li, N.; Ping, Q.; Lu, P.; Zhang, J. Insecticidal characteristics and mechanism of a promising natural insecticide against saw-toothed grain beetle. *RSC Adv.* **2022**, *12*, 7066−7074.
(29) Ersoy, O.; Rençberoğlu, M.; Karapınar Güler, D.; Özkaya, Ö. F. A. Novel flux that determines the physico-chemical properties of calcined diatomite in its industrial use as a filler and filter Aid: Thenardite (Na_2SO_4). *Crystals* **2022**, *12*, 503−518.
(30) Xu, W.; Wang, G.; Xu, J.; Liu, Y.; Chen, R.; Yan, H. Modification of diatomite with melamine coated zeolitic imidazolate framework-8 as an effective flame retardant to enhance flame retardancy and smoke suppression of rigid polyurethane foam. *J. Hazard. Mater.* **2019**, *379*, No. 120819.
(31) Hu, L.; Chen, L.; Fang, Y.; Wang, A.; Chen, C.; Yan, Z. Facile synthesis of zeolitic imidazolate framework-8 (ZIF-8) by forming imidazole-based deep eutectic solvent. *Microporous Mesoporous Mater.* **2018**, *268*, 207−215.
(32) Yang, K.; Yan, L. G.; Yang, Y. M.; Yu, S. J.; Shan, R. R.; Yu, H. Q.; Du, B. Adsorptive removal of phosphate by Mg−Al and Zn−Al layered double hydroxides: kinetics, isotherms and mechanisms. *Sep. Purif. Technol.* **2014**, *124*, 36−42.
(33) Aguedal, H.; Iddou, A.; Aziz, A.; Shishkin, A.; Ločs, J.; Juhna, T. Effect of thermal regeneration of diatomite adsorbent on its efficacy for removal of dye from water. *Int. J. Environ. Sci. Technol.* **2019**, *16*, 113−124.
(34) Al-Musawi, T. J.; Mengelizadeh, N.; Al-Rawi, O.; Balarak, D. Capacity and modeling of acid blue 113 dye adsorption onto chitosan magnetized by Fe_2O_3 nanoparticles. *J. Polym. Environ.* **2022**, *30*, 344−359.
(35) Yusan, S.; Gok, C.; Erenturk, S.; Aytas, S. Adsorptive removal of thorium (IV) using calcined and flux calcined diatomite from Turkey: Evaluation of equilibrium, kinetic and thermodynamic data. *Appl. Clay Sci.* **2012**, *67-68*, 106−116.
(36) Du, Y.; Wang, L.; Wang, J.; Zheng, G.; Wu, J.; Dai, H. Flower-, wire-, and sheet-like MnO_2-deposited diatomites: Highly efficient absorbents for the removal of Cr(VI). *J. Environ. Sci.* **2015**, *29*, 71−81.
(37) Du, Y.; Wang, X.; Wu, J.; Qi, C.; Li, Y. Adsorption and photoreduction of Cr(VI) via diatomite modified by Nb_2O_5 nanorods. *Particuology* **2018**, *40*, 123−130.
(38) Sheng, G.; Hu, J.; Wang, X. Sorption properties of Th (IV) on the raw diatomite-Effects of contact time, pH, ionic strength and temperature. *Appl. Radiat. Isot.* **2008**, *66*, 1313−1320.
(39) Li, S.; Li, D.; Su, F.; Ren, Y.; Qin, G. Uniform surface modification of diatomaceous earth with amorphous manganese oxide and its adsorption characteristics for lead ions. *Appl. Surf. Sci.* **2014**, *317*, 724−729.
(40) Liu, M. M.; Lv, W. M.; Shi, X. F.; Fan, B. B.; Li, R. F. Characterization and catalytic performance of zeolitic imidazolate framework-8 (ZIF-8) synthesized by different methods. *Chin. J. Inorg. Chem.* **2014**, *30*, 579−584.
(41) He, M.; Yao, J.; Liu, Q.; Wang, K.; Chen, F.; Wang, H. Facile synthesis of zeolitic imidazolate framework-8 from a concentrated aqueous solution. *Microporous Mesoporous Mater.* **2014**, *184*, 55−60.
(42) Bustamante, E. L.; Fernández, J. L.; Zamaro, J. M. Influence of the solvent in the synthesis of zeolitic imidazolate framework-8 (ZIF-8) nanocrystals at room temperature. *J. Colloid Interface Sci.* **2014**, *424*, 37−43.
(43) Zhang, B.; Chen, N.; Feng, C.; Zhang, Z. Adsorption for phosphate by crosslinked/non-crosslinked-chitosan-Fe (III) complex sorbents: Characteristic and mechanism. *Chem. Eng. J.* **2018**, *353*, 361−372.
(44) Du, X.; Han, Q.; Li, J.; Li, H. The behavior of phosphate adsorption and its reactions on the surfaces of Fe−Mn oxide adsorbent. *J. Taiwan Inst. Chem. Eng.* **2017**, *76*, 167−175.
(45) Chen, J.; Yan, L.; Yu, H.; Li, S.; Qin, L.; Liu, G.; Li, Y.; Du, B. Efficient removal of phosphate by facile prepared magnetic diatomite and illite clay from aqueous solution. *Chem. Eng. J.* **2016**, *287*, 162−172.
(46) Wang, J.; Zhang, G.; Qiao, S.; Zhou, J. Magnetic fe^0/iron oxide-coated diatomite as a highly efficient adsorbent for recovering phosphorus from water. *Chem. Eng. J.* **2021**, *412*, No. 128696.
(47) Park, J.; Oh, M. Construction of flexible metal-organic framework (MOF) papers through MOF growth on filter paper and their selective dye capture. *Nanoscale* **2017**, *9*, 12850−12854.
(48) Dong, S.; Ji, Q.; Wang, Y.; Liu, H.; Qu, J. Enhanced phosphate removal using zirconium hydroxide encapsulated in quaternized cellulose. *J. Environ. sci.* **2019**, *89*, 102−112.
(49) Li, R.; Wang, J. J.; Zhou, B.; Awasthi, M. K.; Ali, A.; Zhang, Z.; Gaston, L. A.; Lahori, A. H.; Mahar, A. Enhancing phosphate adsorption by Mg/Al layered double hydroxide functionalized biochar with different Mg/Al ratios. *Sci. Total Environ.* **2016**, *559*, 121−129.
(50) Ayranci, E.; Duman, O. Structural effects on the interactions of benzene and naphthalene sulfonates with activated carbon cloth during adsorption from aqueous solutions. *Chem. Eng. J.* **2010**, *156*, 70−76.
(51) Duman, O.; Ayranci, E. Adsorptive removal of cationic surfactants from aqueous solutions onto high-area activated carbon cloth monitored by in situ UV spectroscopy. *J. Hazard. Mater.* **2010**, *174*, 359−367.
(52) Balarak, D.; Zafariyan, M.; Igwegbe, C. A.; Onyechi, K. K.; Ighalo, J. O. Adsorption of acid blue 92 dye from aqueous solutions by single-walled carbon nanotubes: isothermal, kinetic, and thermodynamic studies. *Environ. Process.* **2021**, *8*, 869−888.
(53) Sillanpää, M.; Mahvi, A. H.; Balarak, D.; Khatibi, A. D. Adsorption of acid orange 7 dyes from aqueous solution using polypyrrole/nanosilica composite: Experimental and modelling. *Int. J. Environ. Anal. Chem.* **2021**, 1.
(54) Duman, O.; Tunç, S.; Polat, T. G. Determination of adsorptive properties of expanded vermiculite for the removal of C. I. basic red 9 from aqueous solution: kinetic, isotherm and thermodynamic studies. *Appl. Clay Sci.* **2015**, *109-110*, 22−32.
(55) Duman, O.; Tunç, S.; Polat, T. G. Adsorptive removal of triarylmethane dye (basic red 9) from aqueous solution by sepiolite as effective and low-cost adsorbent. *Microporous Mesoporous Mater.* **2015**, *210*, 176−184.
(56) Wang, S.; Lee, Y. N.; Nam, H.; Nam, H.; Kim, H. K. Chemical activation of porous diatomite ceramic filter for the adsorption of TMA, H_2S, CH_3COOH and NH_3: Isotherm and kinetic studies. *J. Environ. Chem. Eng.* **2019**, *7*, No. 103481.
(57) Al-Musawi, T. J.; Mahvi, A. H.; Khatibi, A. D.; Balarak, D. Effective adsorption of ciprofloxacin antibiotic using powdered activated carbon magnetized by iron(III) oxide magnetic nanoparticles. *J. Porous Mater.* 2021, *28*, 835−852, DOI: 10.1007/s10934-021-01039-7.

https://doi.org/10.1021/acsomega.2c01648
ACS Omega 2022, 7, 26154−26164

(58) Saini, A.; Maheshwari, P. H.; Tripathy, S. S.; Waseem, S.; Dhakate, S. R. Processing of rice straw to derive carbon with efficient de-fluoridation properties for drinking water treatment. *J. Water Process Eng.* **2020**, *34*, 101136−101150.
(59) Dada, A. O.; Olalekan, A. P.; Olatunya, A. M.; Dada, O. Langmuir, Freundlich, Temkin and Dubinin−Radushkevich isotherms studies of equilibrium sorption of Zn^{2+} unto phosphoric acid modified rice husk. *IOSR J. Appl. Chem.* **2012**, *3*, 38−45.
(60) Lu, M.; Zhang, Y.; Guan, X.; Xu, X.; Gao, T. Thermodynamics and kinetics of adsorption for heavy metal ions from aqueous solutions onto surface amino-bacterial cellulose. *Trans. Nonferrous Met. Soc. China* **2014**, *24*, 1912−1917.

https://doi.org/10.1021/acsomega.2c01648
ACS Omega 2022, 7, 26154−26164